

This is the peer reviewed version of the following article: [A. Baroutaji, S. Lenihan, K. Bryan, Mat.-wiss. u. Werkstofftech. 2017, 48, 1133], which has been published in final form at [<https://doi.org/10.1002/mawe.201700048>]. This article may be used for non-commercial purposes in accordance with Wiley Terms and Conditions for Self-Archiving.

Type: Original Article

**Combination of Finite Element Method and Drucker-Prager Cap
Material Model For Simulation of Pharmaceutical Tableting Process**

A.Baroutaji^{1,2*}, K. Bryan², S. Lenihan¹

Ahmad.baroutaji2@mail.dcu.ie

¹ School of Mechanical, Electrical and Process Engineering, Cork Institute
of Technology, Cork, Ireland

² School of Engineering, Faculty of Science and Engineering, University of
Wolverhampton, Telford, UK

Abstract:

Density-dependent Drucker–Prager Cap (DPC) model is widely used for assessing the compaction behaviour of powders due to its capability of capturing the various phenomena associated with the powder compaction process such as work hardening, nonlinear densification, and frictional and compressible behaviour of the powder.

This paper presents a full description of the DPC model for the compaction behaviour of microcrystalline cellulose (MCC) Avicel PH101 pharmaceutical powder. The experimental calibration process of DPC is detailed and all model parameters are calculated as a function of powder relative density.

Also, the calibrated parameters are implemented in finite element code to perform a numerical simulation of a typical pharmaceutical tablet.

The results showed that the finite element model was able to accurately predict the compaction behaviour of the MCC powder. Furthermore, the FE predictions of stress and density distributions of the powders during the compaction were used to analyse the failure mechanisms associated with tableting.

Keywords:

Tableting, Powder compaction, Finite Element Method, Drucker-Prager Cap model.

1 Introduction

Powder compaction has been widely adopted by many industrial sectors such as pharmaceutical, ceramic and automotive to produce complex and high strength components. As a manufacturing process, the powder compaction can provide many advantages over other manufacturing process such as high flexibility, high material utilisation, relatively low energy consumption, low capital costs. In the pharmaceutical industry, powder compaction is widely used to produce pharmaceutical tablets. Compaction of pharmaceutical powders, commonly called tableting, consists of three main stages: (1) die filling, where a mixture of pharmaceutical powders is delivered into the die cavity via a feed shoe; (2) compaction, where the powder

is pressed inside a die by two punches to produce the tablet; and (3) ejection, where the tablet is ejected from the die by the lower punch.

The powder behaviour during each of these stages has an effect on the properties of final tablet [1]. Despite wide spread adoption of powder compaction for pharmaceutical tablets, a successful tableting process which guaranteeing a robust production of high quality pharmaceutical tablets still remains a significant challenge. The tableting process is associated with many complex phenomena that may lead to undesirable tablet defects such as capping, chipping, lamination and low tensile strength. Avoiding such defects requires a sound understanding of the failure mechanisms and this cannot be achieved by using traditional empirical methods such as Heckel analysis and Kawakita equation, which only consider the punch forces, for assessing the tablet properties. Thus, recently, many researchers [2]–[4] adopted a constitutive model, which is capable of describing the yielding of a particulate material as it is compacted, for more comprehensive assessment of a material's compaction properties.

Since the tablet compaction process involves many physical complicated phenomena such as significant reduction in volumes, strain or work hardening, nonlinear densification due to frictional and compressible behaviour of the powder, and the spring-back behaviour which occurs during decompression and ejection, the constitutive material model should be capable of

representing all of these aforementioned phenomena. There are several constitutive material models which represent the yield surfaces of powders such as Drucker–Prager Cap (DPC) model [5], the Cam–Clay model [6] and the DiMaggio–Sandler model [7]. All of these models were originally adopted from soil mechanics and were utilized to simulate the die compaction of metallic [8], ceramic [9] and recently pharmaceutical powders [10]. However, the Drucker–Prager Cap (DPC) model [5] was the most used model in modelling of the pharmaceutical tablet [11], [12], [13] and [14] due to its capability of representing the various phenomena associated with compaction such as shear flow, densification and hardening.

Besides assessing the compaction properties of a powder, employing of constitutive models encompass many other benefits. The parameters of the constitutive model could be used as input in the Finite Element Model (FEM) to perform a detailed analysis of the local mechanical properties, including stresses and density, evolved during the consolidation of powder in a tableting operation. Normally, such information pertaining to the internal structure of the tablet is not readily available from experimental tests. Therefore, computational modelling is considered a very useful, effective and robustness technique that generates essential information in relation to compact density, elastic deformation during ejection and the strength of the tab-

let. Overall, the finite element modelling of pharmaceutical powders compaction was used by researchers and engineers to:

- Estimate and analyse the stress and density distributions within the tablet where these distributions may influence the mechanical properties, dissolution, drug release, and the potential damage during coating, and transport [11].
- Investigate the effect of punch shape and optimize the compaction tools [15] and [16].
- Explore the tablet failure mechanism and assess the origin of defect or crack formation [1], [15], [17], [12], [18] and [19].
- Estimate the break force of the tablet which can replace the empirical methods currently used in design and development process of pharmaceutical product [20].
- Estimate the temperature evolution during compaction that has a direct effect on compressibility and strength, lubricant efficiency, friction between tools, and ejection force [21].
- Investigate the effect of interaction (i.e. friction) between the powder and compaction tools on the process and tablet structure [22].

Generally, the majority of previous studies on the finite element modelling of pharmaceutical powder have only focused on the direct use of DPC param-

eters in the finite element code without describing the role of such parameters in understanding the compaction behaviour of the powder.

Thus, this work aims to combine DPC model and FEM tools for assessing the compaction properties of a pharmaceutical powder and explaining the tablet failure mechanisms. The DPC model parameters were determined experimentally and then used to construct a finite element model for the tableting process. The finite element model was validated experimentally and used to analyse the stress and density distributions within a tablet which in turn highlighted the main causes of some tablet failure modes.

2 Materials and Methods

2.1 Material

The material tested in this paper is a pharmaceutical excipient known as Microcrystalline Cellulose (MCC) Avicel PH 102 (manufactured by FMC BioPolymer, Cork, Ireland). This excipient is widely used in pharmaceutical tablet formulations. The shapes of MCC particles are irregular, with an average particle size of 100 μm and size distribution between 20 and 200 μm according to the manufacturer's specifications. The loose bulk density of the powder is 0.3 g.cc^{-1} while true density is 1.59 g.cc^{-1} . True density value is important in constitutive model calibrations as it is used to calculate relative density (RD) which is the independent variable for all calculated mechanical properties of the powder.

Magnesium stearate (MgSt) was used to lubricate the die and punch prior to compaction tests in order to reduce the friction between tooling and powder.

2.2 Tableting tools and procedure

INSTRON general testing instrument (Model #8872) equipped with a 20 kN load cell and a 12 mm cylindrical instrumented die was used to compact MCC powder. Flat-faced punches were employed to compress the powders. In order to minimise the influence of the wall frictions, a very small quantity of magnesium-stearate was used to lubricate the die wall and punches prior to each test. A known quantity of MCC powder was slowly filled into the die to ensure the uniform distribution of the powder in the die and then it was compacted by the upper punch. The compression (loading) and decompression (unloading) speed was set to 3 mm.s^{-1} . The load transducer was accurately calibrated to ensure the reliability of experimental data. The parameters of the upper punch displacement, upper punch force, and radial pressure were measured every 0.1 ms. The tablet was ejected manually by a long soft punch. After ejection, the dimensions and weight of the compacts were measured to calculate their densities. Punches and die were cleaned and wiped using a cloth and ethanol after each compaction test.

2.3 Drucker-Prager Cap (DPC) model

2.3.1 Description of DPC

The DPC model is a pressure-dependant model which assumes that the behaviour of the powder is isotropic. Normally, the DPC model is represented in the hydrostatic pressure stress (P), Mises equivalent stress (q) coordinate system, Figure 1, by two main surfaces:

(i), the shear failure surface (Fs) which describe the main shear flow of the powder under low mean stresses and depends on the cohesion and the internal friction angle, as expressed in Equation (1)

$$Fs(P, q) = q - P \tan \beta - d = 0 \quad (1)$$

Where β is the internal friction angle, d is the cohesion, P and q are the hydrostatic pressure and the Mises equivalent stresses, respectively.

In tablet compaction, P and q are denoted by Equation (2) and (3), respectively.

$$P = \frac{1}{3} (\sigma_z + 2\sigma_r) \quad (2)$$

$$q = |\sigma_z - \sigma_r| \quad (3)$$

Where σ_z is axial stress and σ_r is radial stress, respectively.

(ii), the 'cap' surface Fc which depicts the strain-hardening plastic behaviour of the powder under high mean stresses induced during the compaction process. The FC surface is represented by an elliptical shape with a constant eccentricity, as shown in Equation (4)

$$F_c(P, q) = \sqrt{(P - P_a)^2 + \left(\frac{Rq}{1 + \alpha - \frac{\alpha}{\cos \beta}}\right)^2} - R(d + P_a \tan \beta) = 0 \quad (4)$$

Where R is a cap shape parameter or eccentricity parameter that controls the shape of the cap, α is a transition surface radius that takes a small value (typically 0.01–0.05), and P_a is an evolution parameter.

The transition surface (F_t) does not have any physical meaning. This surface is, i.e. F_t , only used to allow for a smooth transition between the cap (F_c) and the shear (F_s) which is a numerical requirement to facility the application of FEM.

The F_t is mathematically expressed as in Equation (5):

$$F_t(P, q) = \sqrt{(P - P_a)^2 + \left[q - \left(1 - \frac{\alpha}{\cos \beta}\right) \times (d + P_a \tan \beta)\right]^2} - \alpha(d + P_a \tan \beta) = 0 \quad (5)$$

The full description of DPC model requires knowledge of flow rule. The DPC model uses an associated flow potential (G_c) for the cap region and non-associated flow potential (G_s) for the shear line and transition segment. The G_c and G_s flow potentials are expressed as follows in Equation (6) and (7)

$$G_c = \sqrt{(P - P_a)^2 + \left[\frac{Rq}{1 + \alpha - \frac{\alpha}{\cos \beta}} \right]^2} \quad (6)$$

$$G_s = \sqrt{[(P_a - P)\tan\beta]^2 + \left[\frac{q}{1 + \alpha - \frac{\alpha}{\cos \beta}} \right]^2} \quad (7)$$

2.3.2 Model Calibration Procedure

One of the most important features of the DPC model is that it can be easily characterised and calibrated by performing experiments on powders [23], [8], [10] and [1].

Calibration of DPC model means determination of model parameters, i.e. d , β , R , P_b , and P_a which then can be used in finite element code and for assessing the compaction properties of the powder.

In addition to the parameters of DPC model, the elastic parameters (Young's modulus (E) and the Poisson's ratio (ν)) should also be determined. Consideration of the elastic behaviour is of critical importance for successful modelling of the tablet compaction particularly during the de-compaction and ejection stages where most strains are elastic.

In the tablet compaction modelling, the calibration of DPC model can be performed through an experimental procedure using instrumented die compaction equipment, Table1.

During the compaction, the density of powder changes therefore the whole yielding surface changes.

Thus, in order to account for density changing in the constitutive model, a family of DPC yield surfaces is required, Figure 2. All model parameters should be expressed as functions of the state of the material. Relative density parameter (RD), which is the ratio of tablet density to the true density of the powder, was used to express the state of the powder. Thus, all calibration tests were carried out using a series of specimens compacted to different densities in order to obtain the model parameters as functions of relative density (RD).

Parameters of the shear line (Cohesion (d) and internal friction angle (β))

The parameters of shear line are cohesion and internal friction angle. Cohesion is not a direct measure of the binding forces between particles while it is a measure of a compact's shear strength. The internal friction angle is the slope of shear line. These parameters can be obtained by conducting any two out of the following four possible experiments for measuring the tablet strengths: simple tension, pure shear, diametrical compression, and simple

compression. In this investigation, diametrical and compression tests were selected for calculating the shear line parameters. Diametrical breaking test entails breaking a short compact (thin tablets) between two rigid platens in the diametrical direction, Figure 3. The compact should be sufficiently thin in order to satisfy underlying assumptions of the 'Hertz Theory' which is used to calculate the tensile strength. Thickness to diameter (t/D) aspect ratio of less than 1/4 was maintained for all compacts used in this test. The diametrical strength σ_D , also known as tensile strength, is determined from the diametrical breaking force F_D as per Equation (8)

$$\sigma_D = \frac{2F_D}{\pi D t} \quad (8)$$

For axial breaking tests, long cylindrical specimens were first prepared using die compaction. Height to diameter (H/D) aspect ratio of greater than 2/1 was maintained for all samples in order to reduce the end effects in uniaxial compression tests. The specimens were then placed between two rigid platens and pressed till breaking, Figure 4. The compressive strength σ_c can be calculated from the breaking force F_c and cross sectional area as follows

$$\sigma_c = \frac{4F_c}{\pi D^2} \quad (9)$$

Once the tensile and compressive strength are determined, subsequently cohesion and internal friction angle can be calculated using Equation (10) and (11)

$$d = \frac{\sigma_c \sigma_D (\sqrt{13} - 2)}{\sigma_c + 2\sigma_D} \quad (10)$$

$$\beta = \tan^{-1} \left[\frac{3(\sigma_c + d)}{\sigma_c} \right] \quad (11)$$

Parameters of Cap line

The cap line parameters including eccentricity (R), evolution parameter (P_a) and hydrostatic yield stress (P_b) can be calculated through conduction a series of compaction tests in an instrumented die, i.e. die provided with a pressure sensor to record the pressure transmitted to the die wall which known as die-wall pressure (σ_r). The calculation of cap parameters requires knowledge of axial pressure (σ_z) and radial pressure (σ_r) history during the compaction. Assuming a compaction test to produce a tablet with a specific relative density RD, Figure 5, the end of loading phase (point B) is assumed to be on cap line. From the σ_r and σ_z values at B point, the p and q values are determined using equations (2) and (3). The cap parameters, evolution parameter (P_a) and the eccentricity parameter (R), at a specific relative

density (RD) can be calculated using the d , β , p and q parameters at the same RD as follows

$$P_a \quad (12)$$

$$= -\frac{[3q_{(B)} + 4d \tan\beta(1 + \alpha - \alpha/\cos\beta)^2]}{4[(1 + \alpha - \alpha/\cos\beta)^2]} + \sqrt{\frac{9q_{(B)}^2 + 24dq_{(B)}(1 + \alpha - \alpha/\cos\beta)^2 \tan\beta + 8(3P_{(B)}q_{(B)} + 2q_{(B)}^2)[(1 + \alpha - \alpha/\cos\beta)^2]}{4[(1 + \alpha - \alpha/\cos\beta)^2]}}$$

$$R = \sqrt{\frac{2(1 + \alpha - \alpha/\cos\beta)^2}{3q_{(B)}}(P_{(B)} - P_a)} \quad (13)$$

A value of 0.01 was used for (α) in this investigation.

After calculating P_a and R , the hydrostatic yield stress (P_b) can be determined as follows

$$P_b = P_a + R(d + P_a \tan\beta) \quad (14)$$

Hardening law

Since the powders exhibit a strain hardening behaviour during the compaction whereby the volume reduces and the material becomes harder, DPC use a hardening rule to define the dependence of hydrostatic compression yield stress (P_b) on volumetric plastic strain (ε_v^p), as shown in Equation (15):

$$P_b = f(\varepsilon_v^p) \quad (15)$$

The volumetric plastic strain is given by Equation (16)

$$\varepsilon_v^p = \ln(RD/RD_o) \quad (16)$$

Where RD and RD_o are the final and initial relative densities, respectively. From the instrumented compaction tests used to calculate cap parameters, subsequently P_b and ε_v^p values can be determined in each test and then the hardening law could be established.

Elastic Parameters

The final powder behaviour which should be included in the constitutive model is elasticity. In general, the experimental investigations on the pharmaceutical powders have deduced that powders offered nonlinear elastic behaviour during the unloading phase of the compaction process because of powder dilation phenomena [11]. However, similar to [26], a linear elastic behaviour was assumed for the powder used in the current investigation for more convenient extracting of the elastic parameters. The elastic properties of the powder can be expressed by Young's modulus (E) and the Poisson's ratio (ν). These parameters can be determined from an instrumented compaction test during the unloading phase (BC line in Figure 5). The Young's modulus (E) and the Poisson's ratio (ν) can be calculated in terms of shear modulus K and the bulk modulus G as follows

$$E = \frac{9GK}{3K + G} \quad (17)$$

$$\vartheta = \frac{3K - 2G}{2(3K + G)} \quad (18)$$

The shear and bulk modulus can be determined from the unloading curve as follows

$$K + \frac{3}{4}G = \frac{\sigma_{z(B)} - \sigma_{z(C)}}{\varepsilon_{z(B)} - \varepsilon_{z(C)}} \quad (19)$$

$$\frac{2G}{\sqrt{3}K} = \frac{q_{(B)}}{P_{(B)} - P_{(C)}} \quad (20)$$

Where σ_z , ε_z are axial stress and axial strain, respectively.

B, C represent the states of the powder at the start and end of unloading curve, Figure 5.

2.3.3 Frictions in powder compaction process

During tablet compaction, the friction between the pharmaceutical powders and die wall induces non uniform axial stresses which lead to density gradients inside the tablet. The high friction may cause many undesirable problems such as significant density variations inside the tablet, increased compression and ejection forces, and wear of die wall [24]. Thus, the die wall friction should be kept at minimal levels. To achieve low frictions, lubricant should be used during the compaction process.

Two lubrication methods are predominately used in pharmaceutical industry: (1) internal lubrication method where a lubricant, mostly magnesium

stearate (MgSt), is mixed with the pharmaceutical powders, and (2) external lubrication method which involve spreading the lubricant on the die wall. The friction between the powders and die wall is normally expressed by friction coefficient. The accurate determination of friction coefficient is vital for the computational modelling of powder compaction. Measuring wall friction can be performed by pressing the powder in an instrumented die which has a radial pressure sensor. Based on Janssen-Walker theory, the friction coefficient can be calculated as in Equation (21)

$$\mu = \frac{D}{4h} \frac{\sigma_B}{\sigma_r} \left(\frac{\sigma_T}{\sigma_B} \right)^{\frac{z}{h}} \ln \left(\frac{\sigma_T}{\sigma_B} \right) \quad (21)$$

Where D is the die interior diameter, H is the compaction height in the die, σ_r is the radial pressure at the position z from the top surface of the powder, and σ_B and σ_T are axial compression stresses applied by the upper and lower punches, respectively. Once the friction coefficient is determined, it can be incorporated in the FE code for representing the friction during compaction. In this study, no experimental work was performed to determine the friction coefficient and a value of $\mu=0.1$ was used for FEM Modelling [16], [25].

2.4 Finite element modelling

A commercial finite element package, ABAQUS (Dassault Systèmes, Vélizy-Villacoublay, France), was employed for creating the FE models of

the die compaction of pharmaceutical powders. The finite element model consists of the upper and bottom punches, die walls, and the powder bed, Figure 6. The upper punch was modelled as a rigid body and constrained to move vertically along the y-axis. The bottom punch and die walls were also modelled as rigid entities with all rotations and translations being fixed. The powders were modelled as continuum media by using a 2D-axisymmetric stress element (CAX4R) that has four nodes. Elastic–plastic material model with Drucker–Prager Cap yield surface was employed to represent the behaviour of the powder during the compaction. A hardening mechanism was used to include the hardening behaviour of the powder during the process. The user subroutine “USDFLD” was developed to update the material properties in relation to relative density changes. A surface to surface contact type with finite sliding formulation was employed to define the contact between the powders and compaction tools. A penalty contact option with a friction coefficient value of 0.1 was employed for all contact pairs. This value of friction coefficient was also used by other researchers, [25] and [16], for similar investigation. All models were subjected to axisymmetric boundary conditions in order to reduce simulation solving times. Large strain deformation was included in the finite element model due to the fact that powder experiencing significantly high compaction displacement. The loads were defined by applying the predefined displacement on the

pilot node, which was also used to gather the reaction force from each node.

3 Results and Discussion

3.1 Material parameter identification for the DPC model

3.1.1 Cohesion and Internal friction angle

The axial and diametrical strengths were calculated using Equation (8) and (9), Figure 7. It can be seen that a tablet with higher relative density, i.e. denser tablet, has a higher strength. Also, the magnitude of axial strength is bigger than the diametrical strength for any value of relative density (RD). This observation is consistent with the fact that the shear line should always have a positive slope [26]. After plotting the data points of σ_c and σ_d , a regression analysis was carried out for both strengths to obtain fitting equations to calculate the strengths at any value of RD. Both fitting equations demonstrate high coefficient of determination ($R^2 > 90\%$). The obtained axial and diametrical strengths can be used in equations (10) and (11) to calculate the cohesion and internal friction angle at any value of the relative density. The variation of shear line parameters, i.e. cohesion (d) and internal friction (β), with the relative density (RD) are shown, Figure 8 and 9. Cohesion d increases in an exponential fashion as the powder is densified, Figure 8, while the internal friction angle presents very little dependence on the relative density and is approximately constant, Figure 9.

3.1.2 Cap Parameters

A series of compaction tests in an instrumented die were undertaken to calculate the cap parameters. The changes of axial pressure with axial strain for the conducted tests are measured, Figure 10. The cap parameters are calculated using Equation (12) and (13). Evolution parameter (P_a) and the eccentricity parameter (R) as functions of relative density are calculated, Figure 11 and 12. It is evident that the P_a increases as the relative density increases. This trend infers that a denser tablet requires a higher pressure to start deformation rather than failing in shear. On the other side, the eccentricity parameter is approximately constant with changing the relative density.

3.1.3 Hardening law

The hardening curve is expressed by the hydrostatic yield stress (P_b) as function of the volumetric plastic strains (ϵ_v), Figure 13. Equation (14) and (16) were used to compute P_b and ϵ_v , respectively. The P_b increases exponentially with increasing of ϵ_v , Figure 13.

3.1.4 Elastic Parameters

The elastic parameters represented by Young's modulus (E) and the Poisson's ratio (ν) were determined using Equation (17) and (18).

The Young's modulus of MCC increases rapidly with increasing the relative density, Figure 14. This behaviour demonstrates that a tablet with a higher relative density has higher Young's modulus (E) and hence it will exhibit smaller post compaction recovery during the unloading and ejection phases. The Poisson's ratio (ν) is almost independent of RD, Figure 15, inferring that almost the same magnitude of force is transferred to die walls during compaction. The value is almost 0.16 which illustrates that the radial transmission is low for MCC powder.

3.2 Modelling Results

3.2.1 Mesh convergence and validation of finite element model

A mesh convergence study was performed to determine the optimal element size. Pressure convergence plot of seven different element sizes is shown, Figure 16. It was found that element size of 0.5 mm was able to produce a converged solution within a reasonable period of time.

In order to ensure the accuracy of numerical results, predictions of FE model were validated against experimental data obtained by using INSTRON equipment. The validation was performed by comparing the experimental and predicted axial pressure-axial displacement response, Figure 17. The axial pressure was calculated as the upper punch force divided by the cross section area of the compact. The tooling geometry and quantity of powder

of FE model were the same as those used in experiments presented in 2.3.2.2. A 12 mm cylindrical die and flat-face punches were employed. Initial height of the powder model was set to 12.5 mm corresponding to 4.65 g of powder used in the experiments. It can be seen that the simulation results agree very well with experimental results, Figure 17. This agreement indicates that the constructed finite element model is valid and gives confidence in the predictive capabilities of the proposed model (for tableting).

3.2.2 Stress and density distribution

The density distribution in a tablet is of great importance for assessing the mechanical behaviour of the tablet during the post-compaction process including coating, packaging, and transportation. The spatial distribution of the relative density (RD) at the various stages of compaction is shown, Figure 18. These results were obtained for axial compression pressure of 60 MPa. It can be seen clearly that the compact has a non-homogenous distribution of density due to friction along the die-wall. During all stages of the compression phase, a high density zone is formed at the top rim of the powder, while a low density zone is observed at the bottom edge. This observation is consistent with the experimental and numerical results reported by other researchers [1], [11]. This behaviour is due to fact that the die-wall friction prevents the powder from moving downwards as the upper punch

moves downwards, and this makes the powder around the top corner well compressed while the powder at the bottom corner is less compressed. The low density zone observed at the bottom rim makes the tablet more likely to experience an edge chipping failure at this location during the ejection stage.

The axial stress distribution of the tablets during the various stages of loading and unloading phases is computed, Figure 19. The stress is higher at the top right corner and lower at the bottom corner. At the maximum compaction, the axial stress values varied from 85 MPa to 107 MPa with a relative density from 0.85 to 0.89. At the end of unloading phase, i.e. when removing the upper punch, the stress plot shows region where the sign of the axial stress changes. The regions in the plot with positive sign are risk regions as they are subjected to tension effect and may experience a capping failure during the ejection. These results are consistent to the results reported by other researchers [25].

4 Conclusion

A density-dependent Drucker-Prager was adopted for modelling the mechanical behaviour of MCC pharmaceutical powder during tableting. A full description of the model was given and the experimental calibration procedure was detailed. The model parameters were determined for a pharmaceutical excipient, MCC. A finite element model for the tableting process of

MCC powder was established using ABAQUS/Standard package and USDFLD subroutine to account for the density changes during the process. The predictions of FE model were in good agreement with those results obtained experimentally from a compaction test using an INSTRON machine. The numerical results obtained from FEA including the stress and density distributions proved that they are useful results for analysing the tablet failure modes such as capping and chipping.

Acknowledgment

The authors would like to thank The Pharmaceutical Manufacturing Technology Centre (PMTc) in Ireland for funding this work.

References

- [1]C. Y. Wu, O. M. Ruddy, a. C. Bentham, B. C. Hancock, S. M. Best, and J. a. Elliott, *Powder Technol.***2005**, 152, 107.
- [2]K. LaMarche, D. Buckley, R. Hartley, F. Qian, and S. Badawy, *Powder Technol.* **2014**, 267, 208.
- [3]B. Mitra, J. Hilden, and J. D. Litster, *Powder Technol.* **2016**, 291, 328.
- [4]B. Mitra, J. Hilden, and J. D. Litster, *Powder Technol.* **2016**, 291, 487.
- [5]D. Drucker and W. Prager, *Q. Appl. Math.***1952**, 10, 157.
- [6]A. N. Schofield and C. P. Wroth, *Critical State Soil Mechanics*, McGraw-Hill, London, **1968**.
- [7]F. L. DiMaggio and I. S. Sandler, *J. Eng. Mech. Div.***1970**, 97, 935.

- [8] O. Coube and H. Riedel, *Powder Metall.* **2000**, 43, 123.
- [9] İ. Aydın, B. J. Briscoe, and K. Y. Şanlıtürk, *Powder Technol.* **1996**, 89, 239.
- [10] a. Michrafy, D. Ringenbacher, and P. Tchoreloff, *Powder Technol.* **2002**, 127, 257.
- [11] L. H. Han, J. a. Elliott, a. C. Bentham, A. Mills, G. E. Amidon, and B. C. Hancock, *Int. J. Solids Struct.* **2008**, 45, 3088.
- [12] G. R. Klinzing, A. Zavaliangos, J. Cunningham, T. Mascaro, and D. Winstead, *Comput. Chem. Eng.* **2010**, 34, 1082.
- [13] H. Diarra, V. Mazel, V. Busignies, and P. Tchoreloff, *Int. J. Pharm.* **2015**, 493, 121.
- [14] V. Mazel, H. Diarra, V. Busignies, and P. Tchoreloff, *J. Pharm. Sci.* **2015**, 104, 4339.
- [15] M. S. Kadiri and A. Michrafy, *Powder Technol.* **2013**, 239, 467.
- [16] A. Krok, M. Peciar, and R. Fekete, *Particuology* **2014**, 16, 116.
- [17] C. Y. Wu, B. C. Hancock, A. Mills, a. C. Bentham, S. M. Best, and J. a. Elliott, *Powder Technol.* **2008**, 181, 121.
- [18] S. Garner, E. Ruiz, J. Strong, and A. Zavaliangos, *Powder Technol.* **2014**, 264, 114.

- [19] R. Furukawa, Y. Chen, A. Horiguchi, K. Takagaki, J. Nishi, A. Konishi, Y. Shirakawa, M. Sugimoto, and S. Narisawa, *Int. J. Pharm.* **2015**, 493, 182.
- [20] C. Shang, I. C. Sinka, and J. Pan, "Modelling of the break force of tablets under diametrical compression," *Int. J. Pharm.* **2013**, 445, 99.
- [21] A. Krok, P. García-Triñanes, M. Peciar, and C.-Y. Wu, *Chem. Eng. Res. Des.* **2016**, 110, 141.
- [22] I. C. Sinka, J. C. Cunningham, and A. Zavaliangos, *Powder Technol.* **2003**, 133, 33.
- [23] I. Aydin, B. J. Briscoe, and N. Ozkan, *MRS Bull.* **2013**, 22, 45.
- [24] I. Sinka, *Knowl. Creat. Diffus. Util.* **2007**, 25, 4.
- [25] H. Diarra, V. Mazel, A. Boillon, L. Rehault, V. Busignies, S. Bureau, and P. Tchoreloff, *Powder Technol.* **2012**, 224, 233.
- [26] J. C. Cunningham, I. C. Sinka, and A. Zavaliangos, *J. Pharm. Sci.* **2004**, 93, 2022.

Figure1. Drucker–Prager Cap material model

Figure 2. Family of DPC yield surfaces for various relative densities over the entire range of compaction

Figure 3. Explanation of specimen and test procedure for diametrical breaking test

Figure 4. Explanation of specimen and test procedure for axial breaking test

Figure 5. A typical variation of axial pressure with axial strain during a die compaction of a pharmaceutical powder

Figure 6. 2D-axisymmetric finite element model of the MCC powders

Figure 7. Variation of axial and diametrical strengths with relative density

Figure 8. Variation Cohesion (d) with relative density

Figure 9. Variation of internal friction angle (β) with relative density

Figure 10. Variation of axial pressure with axial strain obtained experimentally for 5 levels of compaction pressure

Figure 11. Variation of evolution with relative density

Figure 12. Variation of eccentricity with relative density

Figure 13. Hydrostatic equivalent yield stress (P_b) as a function of the volume plastic strain (ϵ_v)

Figure 14. Young's modulus as function of relative density

Figure 15. Poisson's ratio as function of relative density

Figure 16. Determination the optimal mesh density: Changes of axial pressure with the mesh element size

Figure 17. Comparison of experimental and numerical results

Figure 18. Relative density (RD) distribution during the various stages of tableting process

Figure 19. Axial stress distribution during the various stages of tableting process

Table 1. Summary of the required experiments for calibrating DPC model

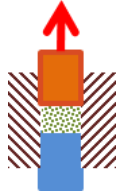
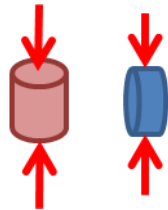
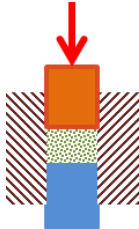
DPC Material Calibration			
Elastic Properties			
E (GPa)	Young's modulus	Instrumented die compaction test, unloading	
ν	Poisson's ratio		
Plastic Properties			
d (MPa)	Cohesion	Uniaxial compression and diametrical compression test	
β	Internal friction angle		
R	Cap shape	Instrumented die compaction test, loading	
Pa	Evolution parameter		
Pb	Hydrostatic yield stress		

Figure1. Drucker–Prager Cap material model

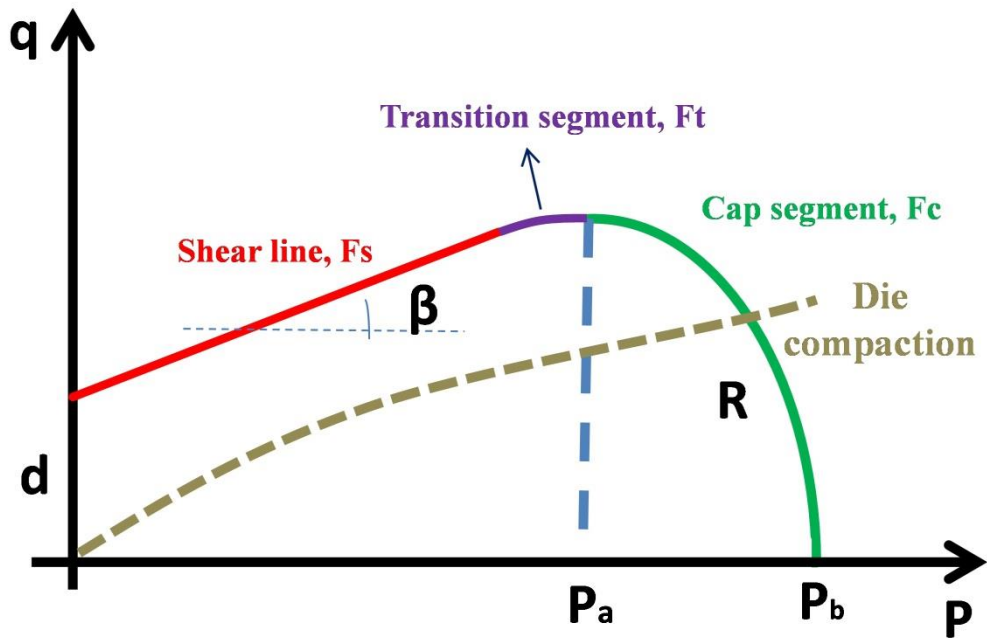


Figure 2. Family of DPC yield surfaces for various relative densities over the entire range of compaction

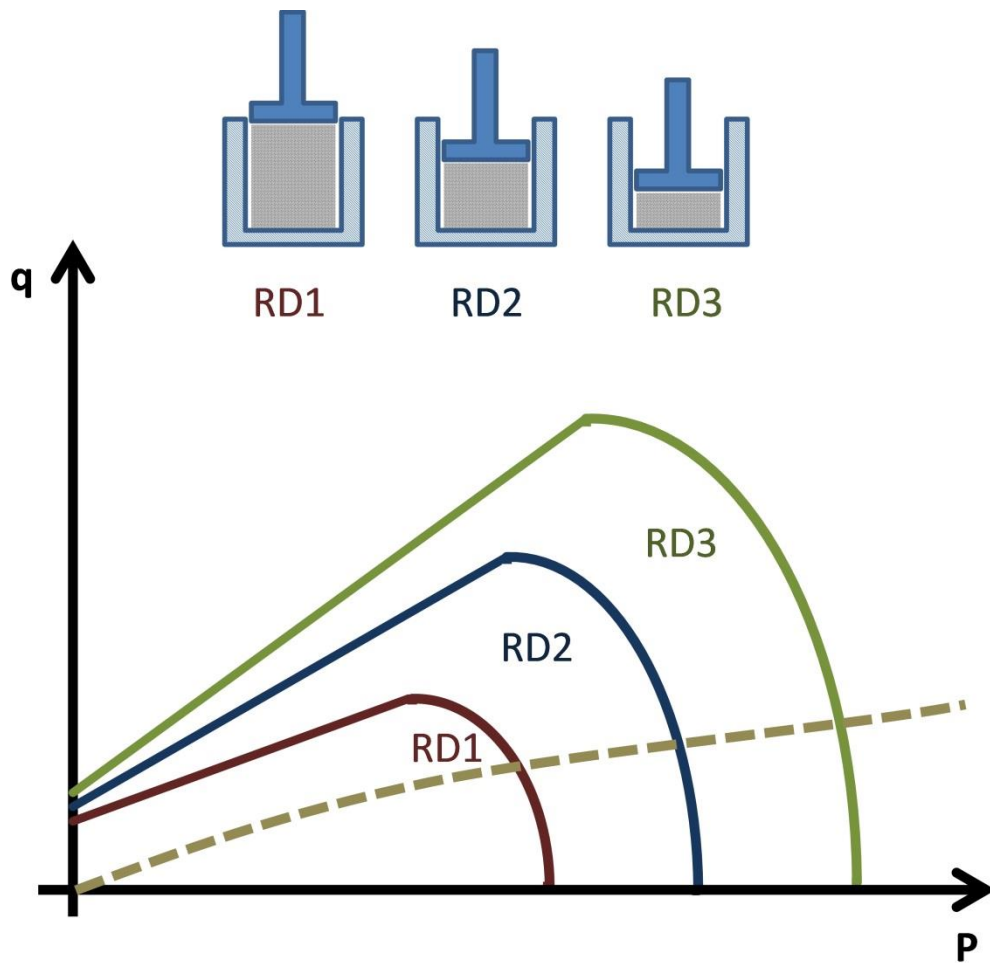


Figure 3. Explanation of specimen and test procedure for diametrical breaking test

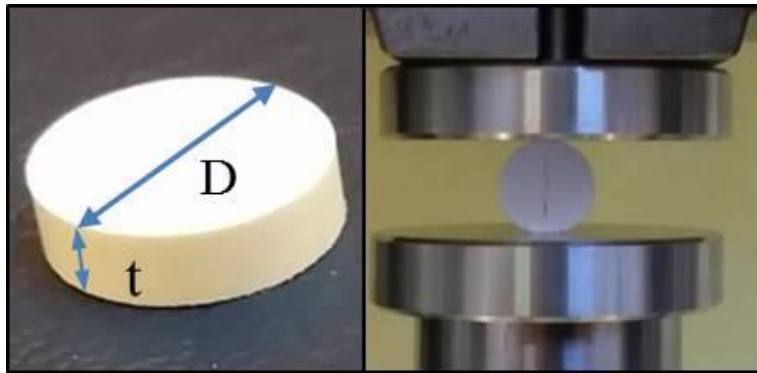


Figure 4. Explanation of specimen and test procedure for axial breaking test

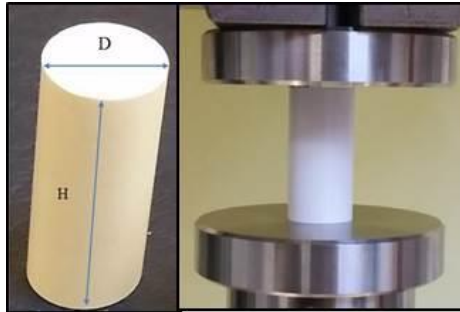


Figure 5. A typical variation of axial pressure with axial strain during a die compaction of a pharmaceutical powder

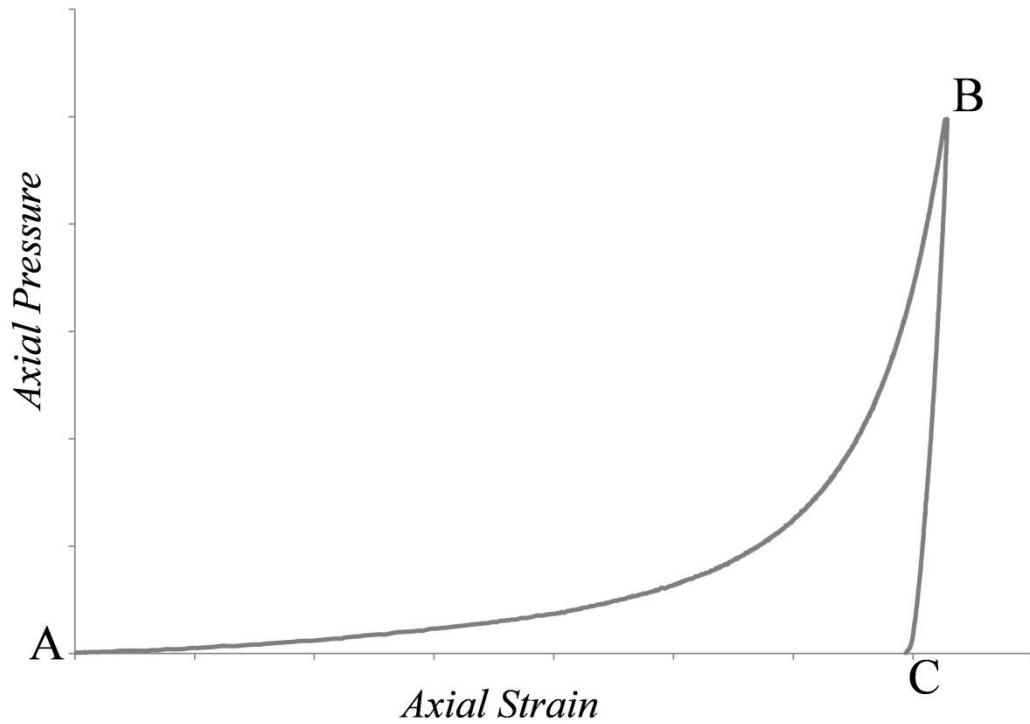


Figure 6. 2D-axisymmetric finite element model of the MCC powders

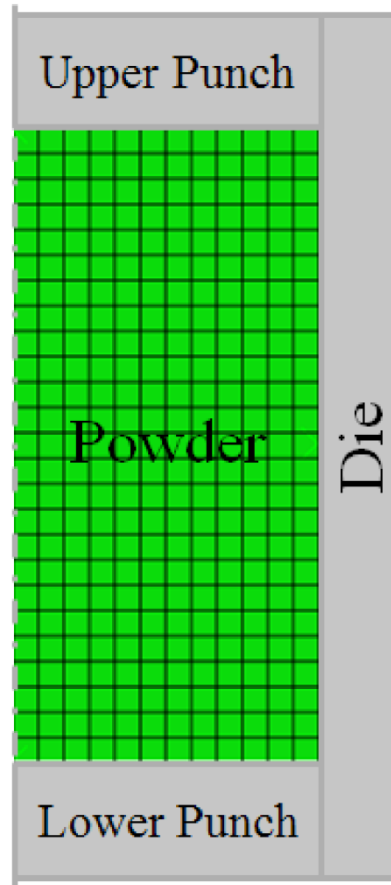


Figure 7. Variation of axial and diametrical strengths with relative density

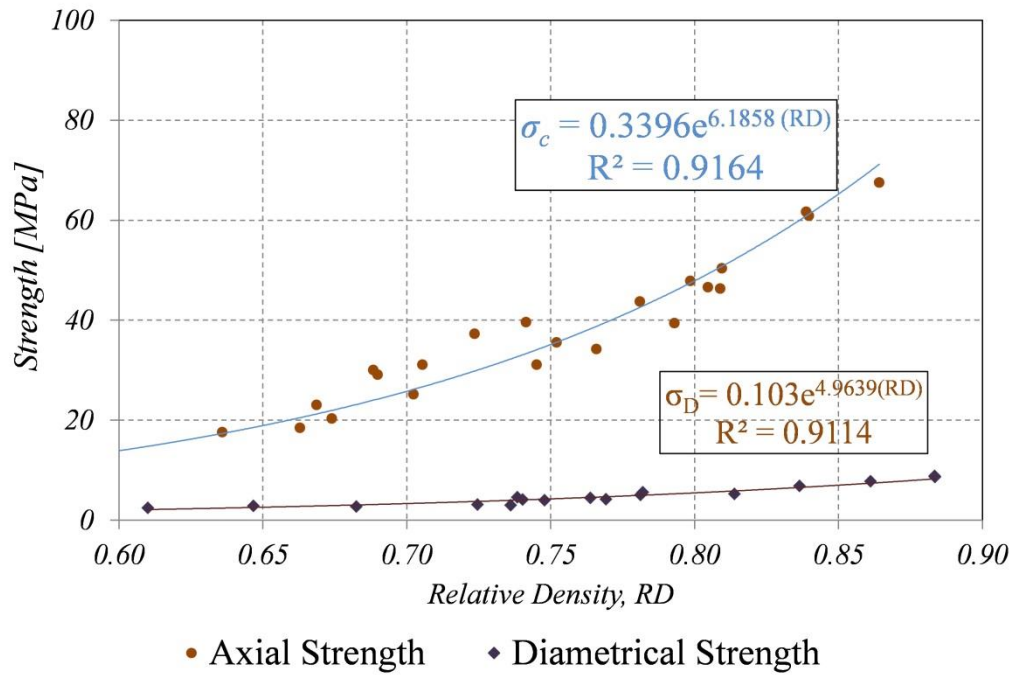


Figure 8. Variation Cohesion (d) with relative density

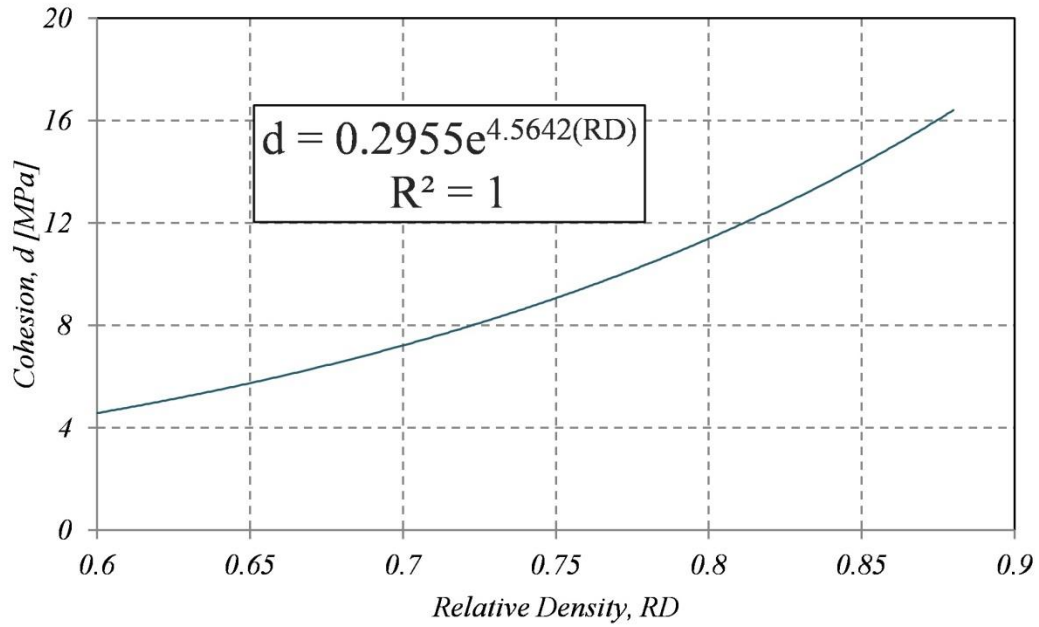


Figure 9. Variation of internal friction angle (β) with relative density

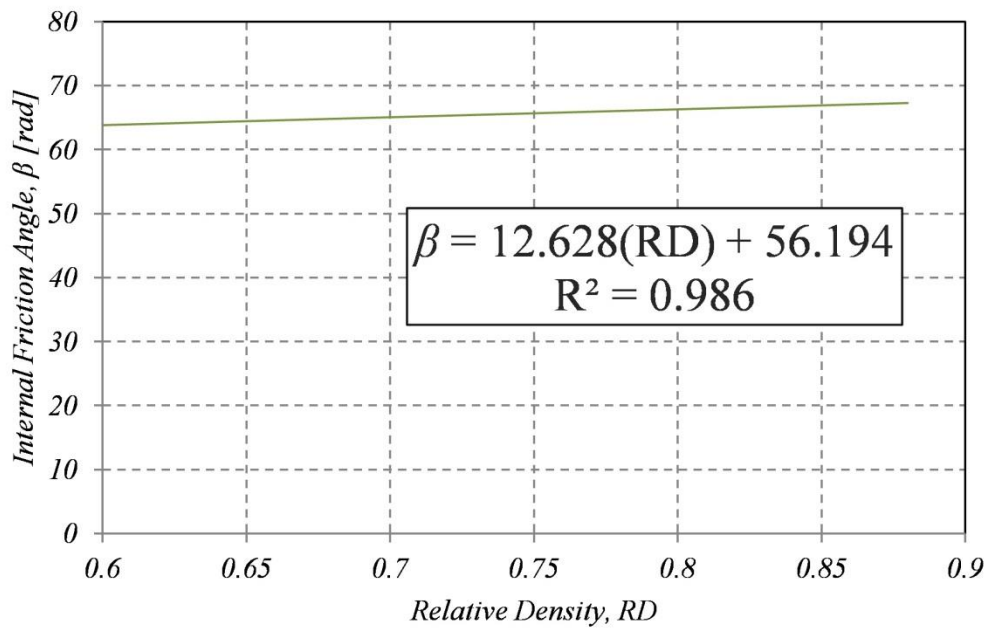


Figure 10. Variation of axial pressure with axial strain obtained experimentally for 5 levels of compaction pressure

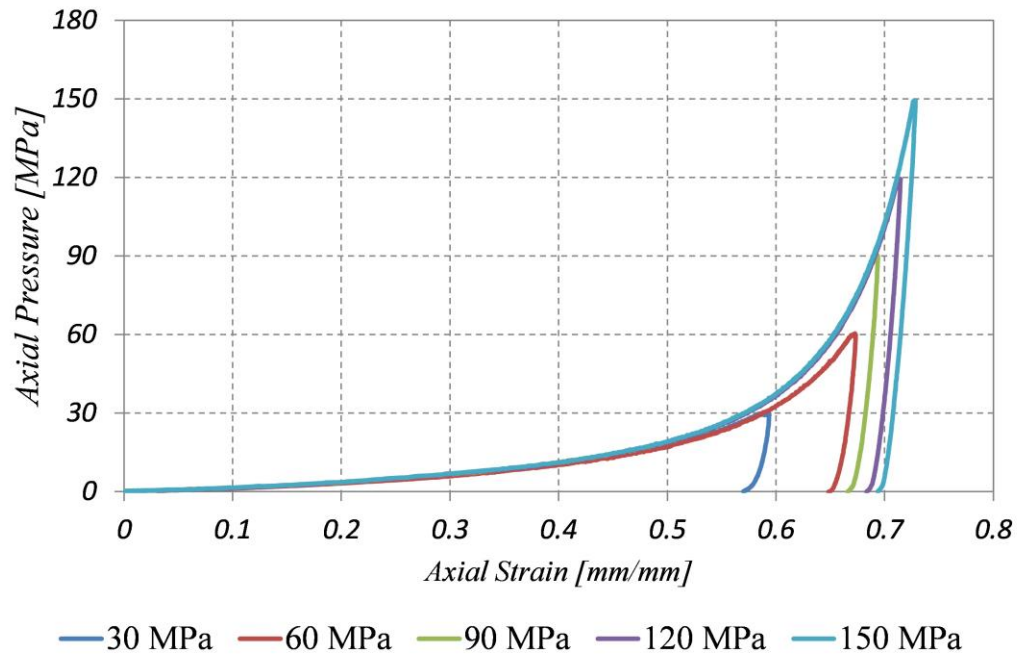


Figure 11. Variation of evolution with relative density

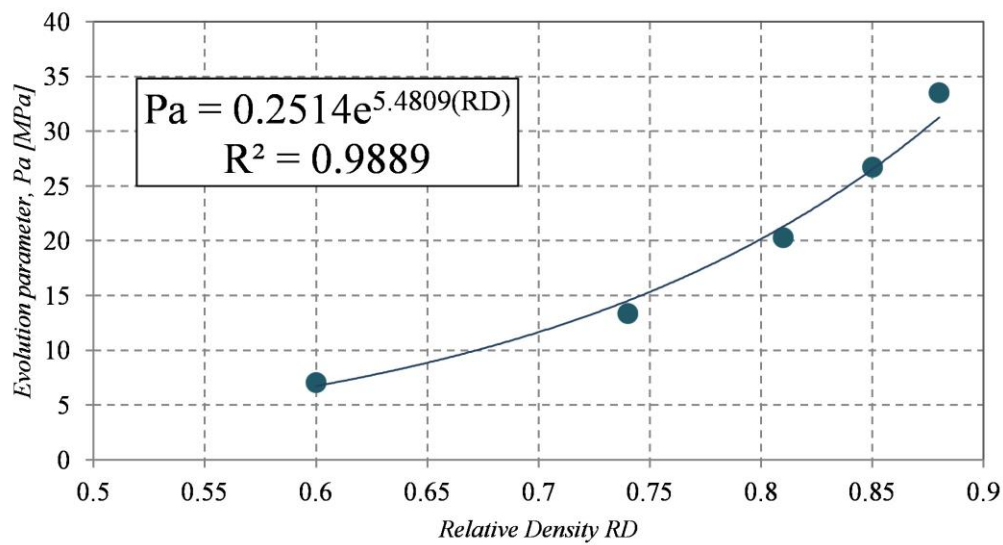


Figure 12. Variation of eccentricity with relative density

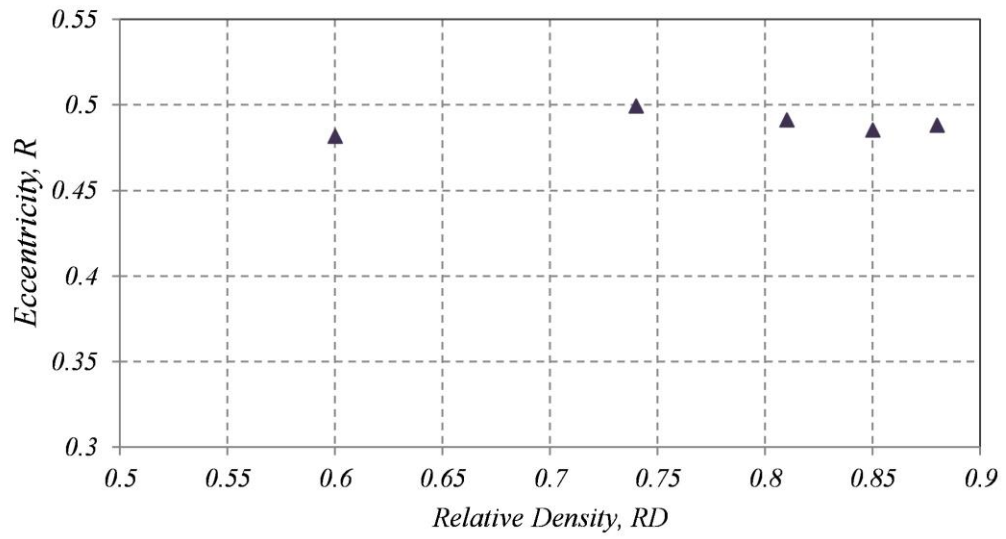


Figure 13. Hydrostatic equivalent yield stress (P_b) as a function of the volume plastic strain (ϵ_v)

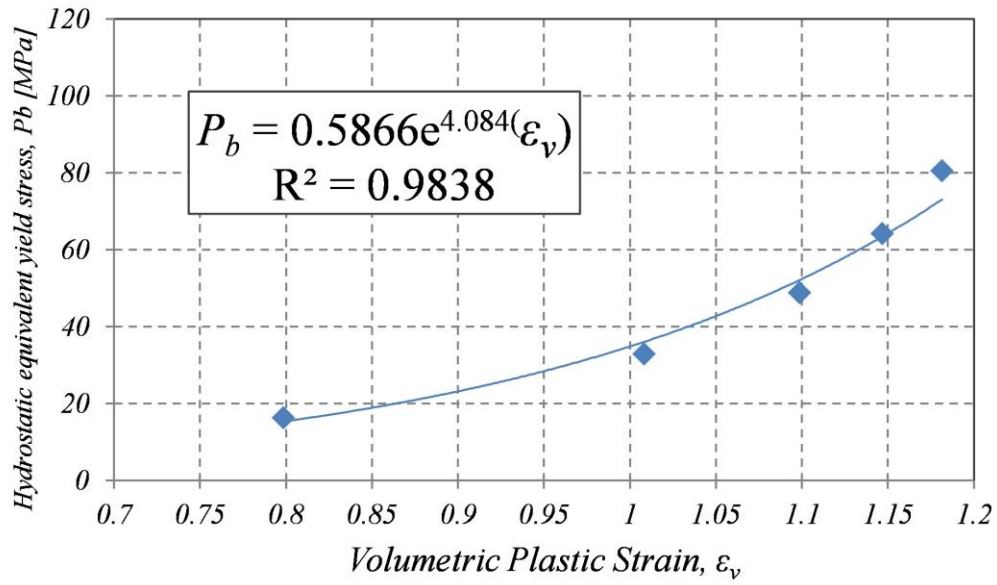


Figure 14. Young's modulus as function of relative density

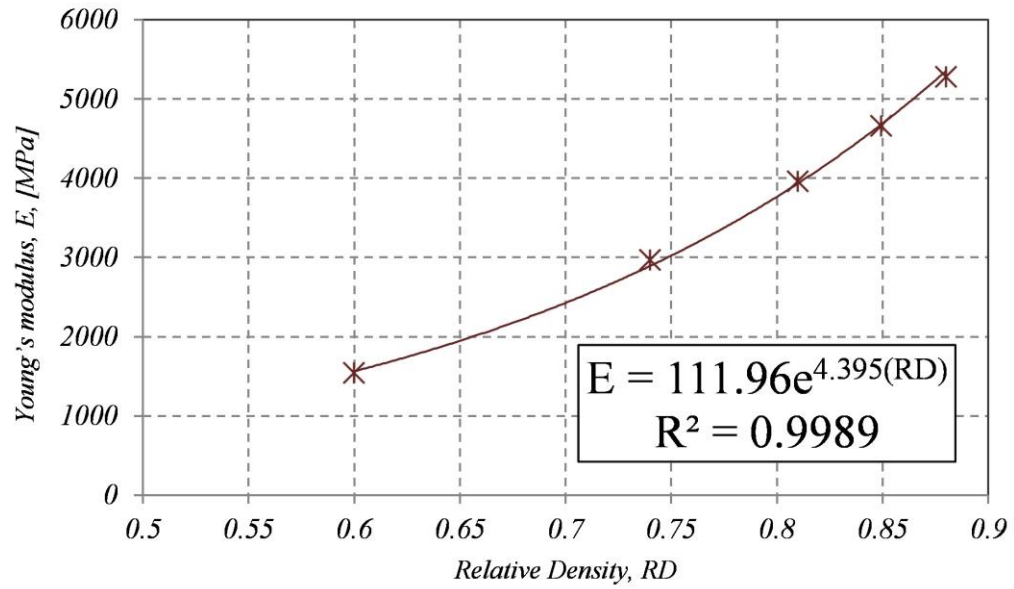


Figure 15. Poisson's ratio as function of relative density

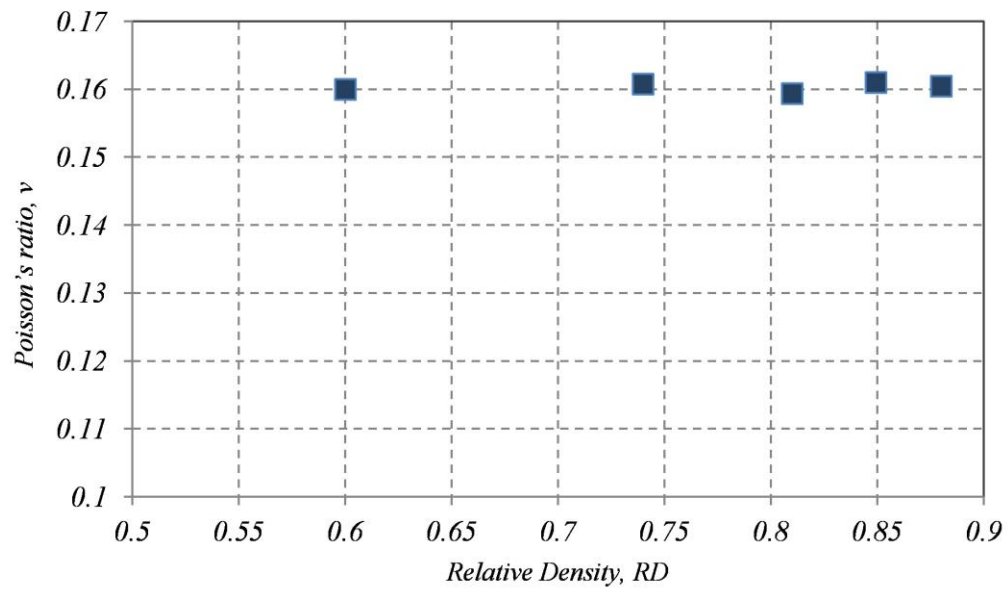


Figure 16. Determination the optimal mesh density: Changes of axial pressure with the mesh element size

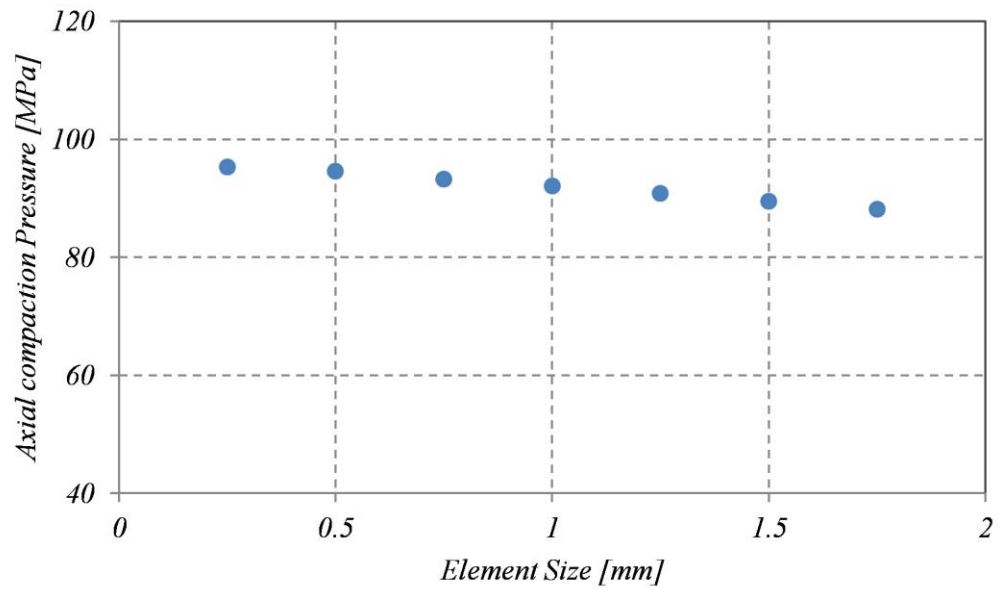


Figure 17. Comparison of experimental and numerical results

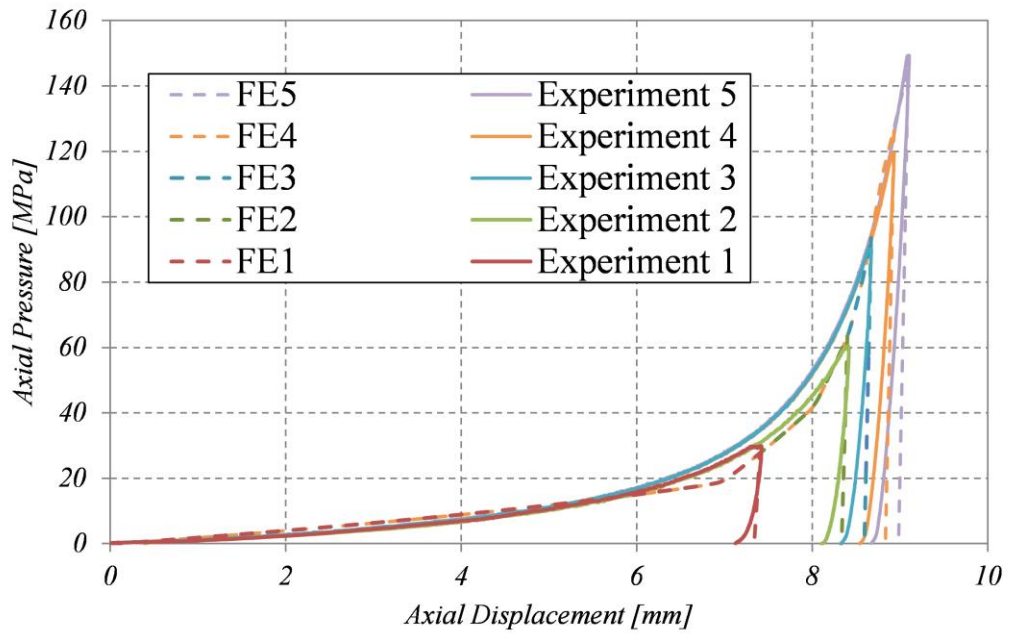


Figure 18. Relative density (RD) distribution during the various stages of
tableting process

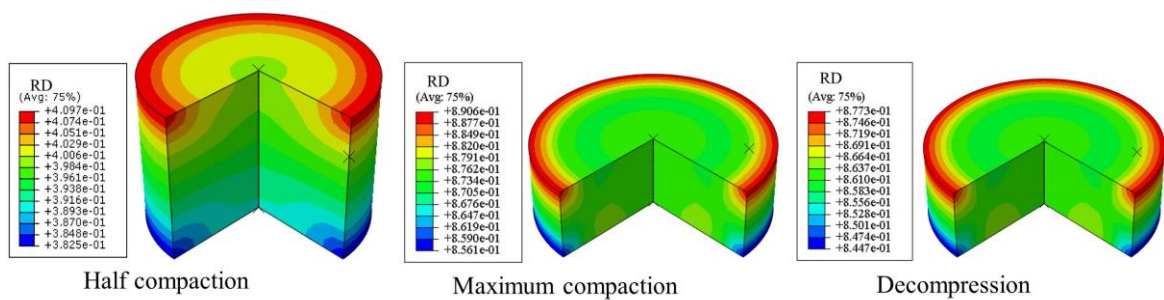


Figure 19. Axial stress distribution during the various stages of tabletting process

